



Contents lists available at ScienceDirect

Bioorganic & Medicinal Chemistry

journal homepage: www.elsevier.com/locate/bmc

Development of cyanopyridine–triazine hybrids as lead multitarget anti-Alzheimer agents

Mudasir Maqbool^a, Apra Manral^b, Ehtesham Jameel^c, Jitendra Kumar^a, Vikas Saini^b, Ashutosh Shandilya^d, Manisha Tiwari^{b,*}, Nasimul Hoda^{a,*}, B. Jayaram^{d,e,f}

^a Department of Chemistry, Jamia Millia Islamia (Central University), Jamia Nagar, New Delhi 110025, India

^b Dr. B. R. Ambedkar Centre for Biomedical Research, University of Delhi, New Delhi 110007, India

^c Department of Chemistry, B. R. Ambedkar Bihar University, Muzaffarpur 842001, Bihar, India

^d Department of Chemistry, Indian Institute of Technology Delhi, Hauz Khas, New Delhi 110016, India

^e Kusuma School of Biological Sciences, IIT Delhi, New Delhi 110016, India

^f Supercomputing Facility for Bioinformatics & Computational Biology, IIT Delhi, New Delhi 110016, India

ARTICLE INFO

Article history:

Received 6 March 2016

Revised 20 April 2016

Accepted 21 April 2016

Available online xxx

Keywords:

Alzheimer's disease

Acetylcholinesterase

Triazine

Molecular docking

Butyrylcholinesterase

Aβ_{1–42} disaggregation

ABSTRACT

A series of new cyanopyridine–triazine hybrids were designed, synthesized and screened as multitargeted anti-Alzheimer's agents. These molecules were designed while using computational techniques and were synthesized via a feasible concurrent synthetic route. Inhibition potencies of synthetic compounds **4a–4h** against cholinesterases, Aβ_{1–42} disaggregation, oxidative stress, cytotoxicity, and neuroprotection against Aβ_{1–42}-induced toxicity of the synthesized compounds were evaluated. Compounds **4d** and **4h** showed promising inhibitory activity on acetylcholinesterase (AChE) with IC₅₀ values 0.059 and 0.080 μM, respectively, along with good inhibition selectivity against AChE over butyrylcholinesterase (BuChE). Molecular modelling studies revealed that these compounds interacted simultaneously with the catalytic active site (CAS) and the peripheral anionic site (PAS) of AChE. The mixed type inhibition of compound **4d** further confirmed their dual binding nature in kinetic studies. Furthermore, the results from neuroprotection studies of most potent compounds **4d** and **4h** indicate that these derivatives can reduce neuronal death induced by H₂O₂-mediated oxidative stress and Aβ_{1–42} induced cytotoxicity. In addition, in silico analysis of absorption, distribution, metabolism and excretion (ADME) profile of best compounds **4d** and **4h** revealed that they have drug like properties. Overall, these cyanopyridine–triazine hybrids can be considered as a candidate with potential impact for further pharmacological development in Alzheimer's therapy.

© 2016 Elsevier Ltd. All rights reserved.

1. Introduction

Alzheimer's disease (AD) is an age-related neurodegenerative disorder, characterized by progressive cognitive impairment, dementia and neuropsychiatric symptoms.^{1,2} It starts with minuscule changes of hippocampal synaptic adequacy, simultaneous

neuronal degeneration, and ultimately death of the patient. It is a chronic disorder that cannot be prevented, cured or slowed hence is the third leading cause of death after cardiovascular diseases and cancer worldwide.

The complete etiology of the disease is still not clear. However, the synaptic dysfunction is believed to be caused due to extracellular amyloid-β (Aβ) aggregation,³ produced by the proteolytic cleavage of a transmembrane protein amyloid precursor protein (APP) by the β- and γ-secretases. Intracellular tangle formation due to hyperphosphorylation of microtubule associated protein tau⁴ which in turn is governed by the overexpression of glycogen synthase kinase beta (GSK-3β),⁵ also accounts for the synaptic dysfunction. These two protein misfoldings are considered to be the main hallmarks of this ailment. Another popular physiological target in AD is cholinergic pathway that tides symptoms of dementia and learning difficulties to the significant decrease of acetylcholine

Abbreviations: ACh, acetylcholine; AChE, acetylcholinesterase; eelAChE, electric eel acetylcholinesterase; BuCh, butyrylcholine; BuChE, butyrylcholinesterase; eqBuChE, equine serum butyrylcholinesterase; ChE, cholinesterase; AD, Alzheimer's disease; Aβ, amyloid beta; AChEI, acetylcholinesterase inhibitor; BChEI, butyrylcholinesterase inhibitor; PAS, peripheral anionic site; CAS, catalytic active site; TcAChE, Torpedo Californica acetylcholinesterase; ROS, reactive oxygen species; SAR, structure activity relationship; SEM, scanning electron microscope; TEM, transmission electron microscopy; ThT assay, thioflavin T assay; equiv, equivalent.

* Corresponding authors.

E-mail addresses: mtiwari07@gmail.com (M. Tiwari), nhoda@jmi.ac.in (N. Hoda).

<http://dx.doi.org/10.1016/j.bmc.2016.04.041>

0968-0896/© 2016 Elsevier Ltd. All rights reserved.

level. AChE, a key member of serine hydrolase family, catalyses the breakdown of acetylcholine (ACh) an important neurotransmitter. Its catalytic triad Ser-His-Glu is located at the bottom of a deep and narrow gorge mainly covered with the aromatic residues which are considered to be responsible for cation- π interaction with the substrate ACh.^{6,7} Peripheral anionic site (PAS) of AChE constitutes Tyr 121, Tyr70 and Trp279 residues, present at the opening of the gorge and guides the substrate approaching the active site. In addition, A β binds to the peripheral anionic site (PAS) of the AChE which enhances the rate of A β fibril formation.^{8,9} Therefore, due to their non-classical roles, cholinesterase inhibitors could also be useful as potential disease-modifying drugs.^{10,11}

On the other hand, evasion of A β stockpile is considered to be the potentially influential step approaching the treatment of AD.¹² In addition to this, oxidative stress occurs in the early breakthrough of AD.¹³ Brain aging is directly correlated to the AD development which in turn is believed to be due to a gradient between production of reactive oxygen species (ROS) and antioxidant defences.¹⁴ Several evidences suggest that oxidative stress has a prominent role in the AD buildup. Therefore, therapeutics targeting clearance or prevention of the free radicals in the brain would be beneficial against AD.

Till date drugs like tacrine, donepezil, rivastigmine, galanthamine, caproctamine and memantine targeting cholinesterases, cholesterol esterase, and lipase are used to treat AD but these drugs only curtail the symptoms and do not produce a complete cure. These drugs are also recognized to have many side effects including hepatotoxicity, gastrointestinal disturbance, dizziness, diarrhoea, vomiting and nausea.^{15,16}

1,3,5-Triazine scaffold has been serving medicinal chemists for a long time for the development of antifungal,¹⁷ anticancer,¹⁸ anti-malarial,¹⁹ antiviral,²⁰ antibacterial agents.²¹ The construction of triazine and its derivatives could be easily achieved by routine chemical reactions.

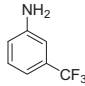
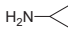
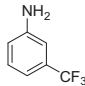
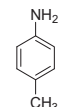
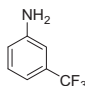
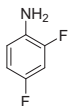
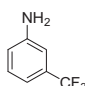
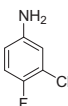
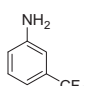
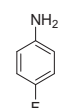
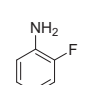
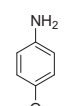
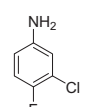
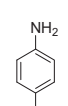
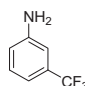
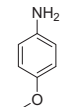
Keeping the above aspects into consideration, here we have designed and synthesized a series of eight new cyanopyridine-triazine hybrids as persuasive multifunctional agents for the treatment of AD. All the synthesized compounds were assessed for their inhibitory activity towards cholinesterases and their A β anti-aggregating activity. Further, the mechanism of AChE inhibition was investigated by kinetic studies. Selected cholinesterase inhibitors were subsequently examined for neuroprotective properties in SH-SY5Y neuronal cells. In order to obtain a better understanding of possible interactions with biological targets, molecular docking studies were also performed.

2. Results and discussion

2.1. Chemistry

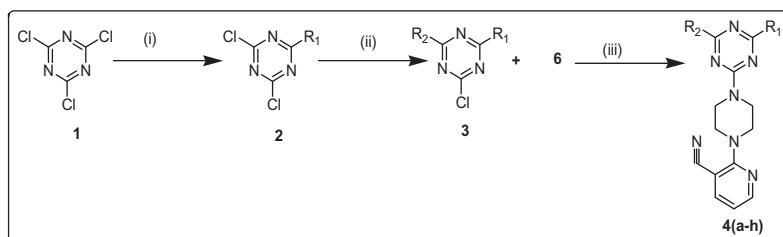
The target molecules were synthesized via multiple steps as depicted in Schemes 1 and 2. The mono and di-substituted triazine compounds (**2a–2h** and **3a–3h**) were synthesized according to the reported literature procedure.²² 2,4,6-Trichloro-1,3,5-triazine was first treated with 3-(trifluoromethyl)aniline (**2a–2e**, **2h**), 2-fluoroaniline (**2f**), 3-chloro-4-fluoroaniline (**2g**) at -10°C in THF and K_2CO_3 . The mono-substituted triazine compounds were further treated with different amines to obtain disubstituted compounds (**3a–3h**). On the other hand, 2-(piperazin-1-yl)nicotinonitrile (**6**) was synthesized as shown in Scheme 2.²³ Finally, the di-substituted triazine compounds (**3a–3h**) were treated with compound (**6**) in presence of K_2CO_3 and 1,4-dioxane at 110°C to obtain the targeted compounds as tri-substituted triazines (**4a–4h**). The reactions involved in the synthesis of the target compounds were temperature dependent nucleophilic aromatic substitution reactions.

The monosubstituted triazines were synthesized at below 0°C , disubstituted at room temperature and the targeted compounds were obtained at higher temperature, i.e., 110°C . All the newly synthesized compounds were purified by column chromatography and were characterized by different spectroscopic techniques— ^1H NMR, ^{13}C NMR, ESI MS and elemental analysis.

Compound	R ₁	R ₂
4a		
4b		
4c		
4d		
4e		
4f		
4g		
4h		

2.2. Design of multifunctional ligands

In order to develop a persuasive drug candidate for multifaceted AD, we undertook structure based drug design approach. Triazine was selected as preferred scaffold, because its roughly planar structure was expected to intercalate between beta-amyloid sheets and was expected to enhance the beta-amyloid disaggregation. It was also expected to engage efficiently with the active site residues of AChE via weak non-covalent interactions like H-bonding, π - π stacking interaction, and alkyl- π -interaction. In addition, the molecules substituted with *p*-anisidine are known to have neuroprotective and radical scavenging capability.²⁴ Inclusion of piperazine was a natural choice to connect two electrophilic centres. Nitrogen of piperazine was expected to be in protonated state and hence may engage in π -cation interactions with the residues of aromatic gorge. Pardock module of Sanjeevini (SCFBIO, IITD)^{25,26}



Scheme 1. Reagents and conditions: (i) aromatic amines, tetrahydrofuran (THF), -110°C , 1–4 h, K_2CO_3 , N_2 (ii) aromatic amines, tetrahydrofuran (THF), rt, 6–12 h, K_2CO_3 , N_2 (iii) 1,4-dioxane, reflux, 12–16 h, K_2CO_3 , N_2 .



Scheme 2. Reagents and conditions: (a) Piperazine, K_2CO_3 , 1,4-dioxane, reflux, 3–4 h, **5** = 2-chloronicotinonitrile.

a comprehensive drug design suite was selected for docking and scoring. The computational binding free energy of synthesized compounds **4a–4h** with AChE and BuChE is mentioned in Table 1. The Binding free energy (ΔG in kcal/mol) of compounds **4d** and **4h** with AChE was found to be -14.41 and -14.13 , respectively, suggesting a very high binding-affinity between the ligands and the enzyme. All the compounds **4a–4h** showed more inhibition selectivity against AChE over BuChE.

Table 1

The calculated free energies of selected derivatives in molecular docking using ParDOCK²⁷

Compound	Calculated free energy (Kcal/mol) AChE	Calculated free energy (Kcal/mol) BuChE
4a	-12.76	-12.14
4b	-12.35	-11.61
4c	-13.20	-11.85
4d	-14.41	-13.40
4e	-12.59	-10.61
4f	-12.12	-10.34
4g	-13.01	-11.48
4h	-14.13	-10.94

Bolded values represent the most active compounds **4d** and **4h**.

A docking study was performed on reported crystal structure of AChE which was retrieved from RCSB (PDB ID 1EVE). Compounds **4d** and **4h** were predicted to show better interaction with AChE. In Figure 1a aromatic ring of Trp279 and Tyr334 was expected to interact with 3-chloro-4-fluoroaniline and triazine moiety via π – π stacking, likewise Phe330 and Phe331 simultaneously with 3-(trifluoromethyl)aniline of compound **4d**. In Figure 1b Phe330 and Phe331 was expected to engage with *p*-anisidine ring of compound **4h** through aryl–aryl interaction. Similarly Trp279 and Tyr334 was supposed to interact with 3-(trifluoromethyl)aniline and triazine rings, respectively. In addition to this, a strong hydrogen bond was assumed between the oxygen of *p*-anisidine and hydrogen of His440 with donor–acceptor distance of 2.42 \AA .

The results of docking study revealed that the dual binding activity for selected compound may be due to π – π (aromatic) and hydrogen bonding interactions with CAS and PAS of AChE.

Docking studies were further extended to the reported crystal structure of Human BuChE (PDB ID 4TPK) with the synthesized compounds. The docked structures of most two potent compounds (**4d** and **4h**) are given in Figure 2a and b, respectively. However, the calculated free binding energies of the synthesized compounds **4a–4h** suggested their selectivity towards AChE over BuChE as shown in Table 1.

2.3. Biology

2.3.1. Inhibitory activity against cholinesterases

The inhibitory activity of synthetic compounds (**4a–4h**) against AChE (from electric eel) and BuChE (from equine serum) was evaluated using the method of Ellman et al.,²⁸ with tacrine and donepezil as a positive control. Their IC_{50} values and selectivity index for AChE over BuChE were summarized as shown in Table 2. Most of the target compounds achieved IC_{50} values in sub-micromolar to nanomolar range with better inhibitory potency towards AChE

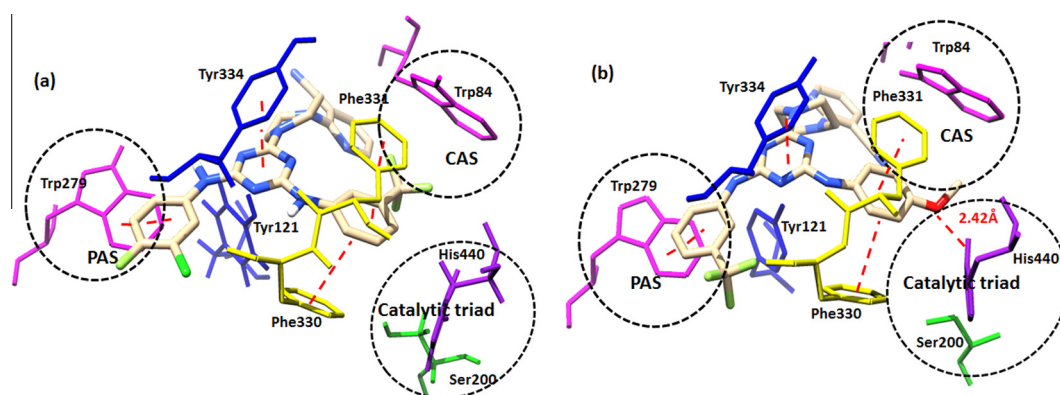


Figure 1. (a) and (b) are the docked structures of compounds **4d** and **4h**, respectively, with AChE. Tyr residues is shown in blue, Phe in yellow, His in purple, Ser in green, and Trp in magenta colours. The π – π stacking between two aryl centres and H-bonding interactions are shown by red coloured dashed lines.

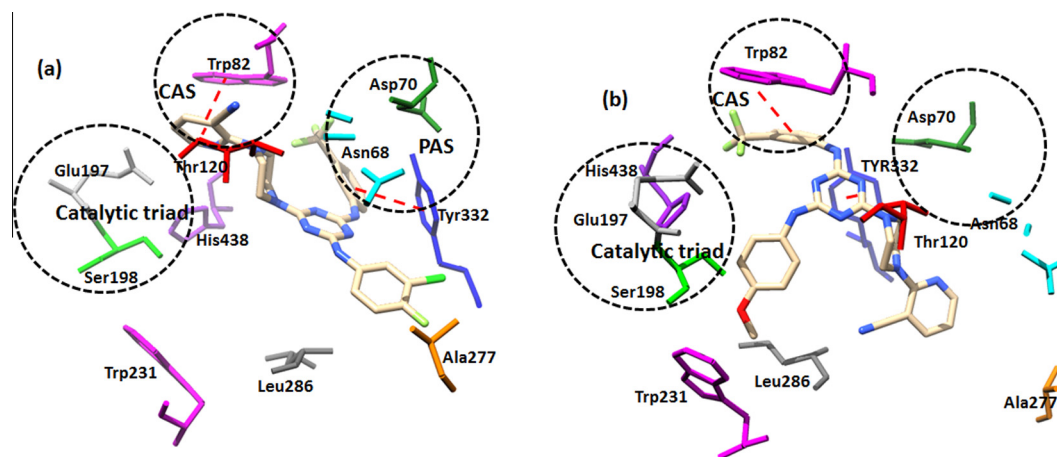


Figure 2. (a) and (b) are the docked structures of compounds **4d** and **4h**, respectively, with BuChE. Tyr residues is shown in blue, His in purple, Ser in green, Leu in dim grey, Ala in orange, Asn in cyan, Asp in forest green, Thr in red, Glu in dark green, and Trp in magentas colours. The π - π stacking interaction between two aryl centres is shown by red coloured dashed lines.

Table 2
In vitro inhibition of AChE and BuChE, selectivity index and oxygen radical absorbance capacity (ORAC, Trolox equivalents) of **4a–4h**, donepezil, and tacrine

Compounds	AChE ^a IC ₅₀ (μ M)	BuChE ^b IC ₅₀ (μ M)	Selectivity ^c BuChE/ AChE	ORAC ^d
4a	0.528 \pm 0.04	5.245 \pm 0.13	9.93	1.03 \pm 0.02
4b	0.153 \pm 0.01	2.214 \pm 0.005	14.47	1.72 \pm 0.05
4c	0.072 \pm 0.02	2.849 \pm 0.09	39.5	2.30 \pm 0.14
4d	0.059 \pm 0.003	3.603 \pm 0.07	61.06	2.39 \pm 0.08
4e	0.084 \pm 0.004	4.894 \pm 0.07	58.26	2.45 \pm 0.04
4f	1.412 \pm 0.02	4.132 \pm 0.007	2.9	2.92 \pm 0.23
4g	1.701 \pm 0.08	5.365 \pm 0.16	3.1	1.89 \pm 0.07
4h	0.080 \pm 0.005	2.015 \pm 0.08	25.2	3.46 \pm 0.15
Donepezil	0.038 \pm 0.001	3.14 \pm 0.2	82.6	n.t
Tacrine	0.13 \pm 0.21	0.054 \pm 0.85	0.40	n.t

Bolded values represent the most active compounds **4d** and **4h**.

n.t—Not tested.

^a 50% inhibitory concentration (means \pm SD of three experiments) of AChE from electric eel.

^b 50% inhibitory concentration (means \pm SD of three experiments) of BuChE from equine serum.

^c SI selectivity index for AChE; IC₅₀ eq BuChE/eelIC₅₀ AChE.

^d Data are expressed as μ mol of trolox equivalent/ μ mol of tested compound.

over BuChE. With the aim of optimizing the inhibitory activity of the synthesized compounds on ChEs, substituents with different electronic properties were varied on core triazine scaffold. Within the series, it was observed that compounds featuring 3-(trifluoromethyl)aniline attached to triazine moiety (compounds **4a–4e** and **4h**), showed stronger inhibition of AChE than 2-fluoro and 3-chloro-4-fluoro containing aniline substituents, i.e., **4f** (IC₅₀ = 1.412 μ M) and **4g** (IC₅₀ = 1.701 μ M), respectively.

Within the sub-group of triazines containing 3-(trifluoromethyl)aniline, it was observed that inhibitory activity against AChE was improved as electron withdrawing properties of 5-(substituted)aniline moiety increased. Thus, the trend observed was as follows: **4c** [5-(2,4-difluoro)aniline] > **4e** [5-(4-fluoro)aniline] > **4h** [5-(4-methoxy)aniline] > **4b** [5-(4-methyl)aniline], respectively. Interestingly, compound **4d** bearing 3-chloro-4-fluoroaniline possessed highest inhibitory potency (IC₅₀ = 0.059 μ M) despite being lesser electronegative than compound **4c**. One likely explanation could be the presence of -Cl group might have contributed in stabilizing the 3-D structure of the pharmacophore and facilitating its interaction with the active site of the enzyme. Furthermore, the replacement of substituted aniline group with cyclopropylamine in compound **4a** lead to a significant loss of inhibitory potency

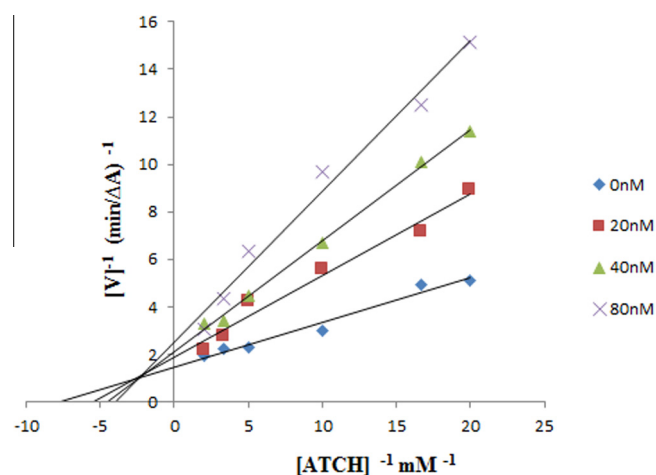


Figure 3. Lineweaver–Burk plots resulting from subvelocity curve of AChE activity with different substrate concentrations (0.05–0.50 mM) in the absence and presence of 20 nM, 40 nM and 80 nM of compound **4d**.

(IC₅₀ = 0.528 μ M) which was nearly 9 folds lower than most potent compound **4d**. It was also worth noting that all the target compounds exhibited greater selectivity towards AChE over BuChE with best derivative **4d** attained selectivity ratio of 61-fold. Moreover, inhibitory potency of **4d** was found to be comparable to standard donepezil (IC₅₀ = 0.038 μ M) and better than tacrine (IC₅₀ = 0.038 μ M). Further, docking studies were carried out with cholinesterases to bring more clarity in understanding their mode of action.

2.3.2. Kinetic study of AChE

To gain further insight into the mechanism of action on AChE of the potent inhibitor **4d**, Lineweaver–Burk double reciprocal plots were generated. The interception of the lines in the Lineweaver–Burk plot above the x-axis with both increased slope (decreased V_{max}) and intercepts (higher K_m) at increasing concentration of the inhibitor, which indicated a mixed-type inhibition. Based on their kinetic studies, we concluded that compound **4d** might be able to interact with both the catalytic active site (CAS) and peripheral anionic site (PAS) of AChE (Fig. 3).

2.3.3. Inhibition of self-mediated A β _{1–42} aggregation

Targeting the self-induced A β _{1–42} aggregation represents an emerging approach for discovering drug candidates for AD.

Table 3Inhibition of self-induced A β_{1-42} aggregation by target compounds **4a–4h** and reference compound curcumin

Compound	A β_{1-42} aggregation inhibition (%) ^a	A β_{1-42} aggregation IC ₅₀ (μ M) ^b
4a	60.7 \pm 0.44	22.4 \pm 0.18
4b	70.5 \pm 0.61	16.7 \pm 0.11
4c	81.2 \pm 0.82	11.3 \pm 0.12
4d	83.7 \pm 1.13	10.1 \pm 0.09
4e	80.4 \pm 0.66	12.8 \pm 0.15
4f	68.5 \pm 0.33	17.4 \pm 0.12
4g	63.5 \pm 0.54	18.9 \pm 0.13
4h	82.4 \pm 1.08	10.9 \pm 0.15
Curcumin	55.3 \pm 0.87	22.84 \pm 0.16

Bolded values represent the most active compounds **4d** and **4h**.^a Inhibition of self-induced A β_{1-42} aggregation (25 μ M) by tested inhibitors at 25 μ M by thioflavin-T based fluorescence method (means \pm SD of three experiments).^b The concentration (μ M) required for 50% inhibition was determined from dose-response curves. Data are expressed as means \pm SD of three independent experiments.

A β_{1-42} has a high tendency to form fibrils and aggregates. Also, its oligomers are neurotoxic and cause membrane disruption in neuronal cells.²⁹ To investigate the activity of our compounds to inhibit the self-mediated A β_{1-42} aggregation, the thioflavin-T (ThT) fluorescence assay was performed.³⁰ As shown in Table 2, most of our compounds showed better inhibitory activity of A β_{1-42} aggregation (1.09–1.5 folds) at 25 μ M compared to the reference compound curcumin. The plausible reason for their remarkable anti-aggregation activity was the presence of core triazine moiety, through which the pharmacophore acquire a nearly planer structure which in turn enables it to fit between the beta-amyloid sheets and thus produced a beta-amyloid disaggregating effect.

Within the group, a similar trend could be seen in the activities of compounds **4a–4h** shown in Table 3, as was observed in cholinesterase inhibition assay. This might be due to the involvement of peripheral anionic site (PAS) site of AChE enzyme, the blockade

of which could interfere with A β aggregation process.³¹ Therefore, the three most potent compounds of the series against A β_{1-42} aggregation **4d** (83.7%, IC₅₀ = 10.1 μ M), **4h** (82.4%, IC₅₀ = 10.9 μ M) and **4c** (81.2%, IC₅₀ = 11.3 μ M) have corresponding higher cholinesterase inhibitory activity as well. Hence, on the basis of in vitro, kinetic and the molecular docking results, we can conclude that the target compounds act as dual binding site AChE inhibitors, endowed with A β anti-aggregating properties.

2.3.4. Antioxidant activity

The antioxidant activities of compounds **4a–4h** were evaluated by the well-established ORAC-FL method.^{32,33} Peroxyl radicals were thermally generated from 2,2-azobis (amidinopropane) dihydrochloride and reacted with fluorescein to form nonfluorescent products at 535 nm. The antioxidant capacity of compounds **4a–4h** was determined by their competition with fluorescein in the radical capture, using a fluorescence microplate reader (Table 1). The ability of compounds **4a–4h** to scavenge radicals at concentrations between 1 and 10 μ M was compared with that of the highly potent compound Trolox and is expressed as its equivalent. All the target compounds exhibited significant radical-capture capacities ranging from 1.03 to 3.46 times the Trolox value. Compounds **4h** however, exhibited the most potent antioxidant activity within the series with ORAC-FL values of 3.46 trolox equivalents followed by compound **4f** with 2.92 trolox equivalents, respectively. The presence of common structural feature, i.e., methoxy substituted moieties, in compounds **4h** and **4f** appears to be favourable to the compound's overall radical scavenging ability.

2.3.5. Inhibition of A β_{1-42} aggregation formation monitored by transmission electron microscopy (TEM)

Finally, transmission electron microscopy (TEM) was employed³⁴ to monitor and clarify the effect of two most potent compounds **4d** and **4h** on A β_{1-42} aggregation along with curcumin as control.³⁵ As shown in Figure 4b, after incubation at 37 °C for

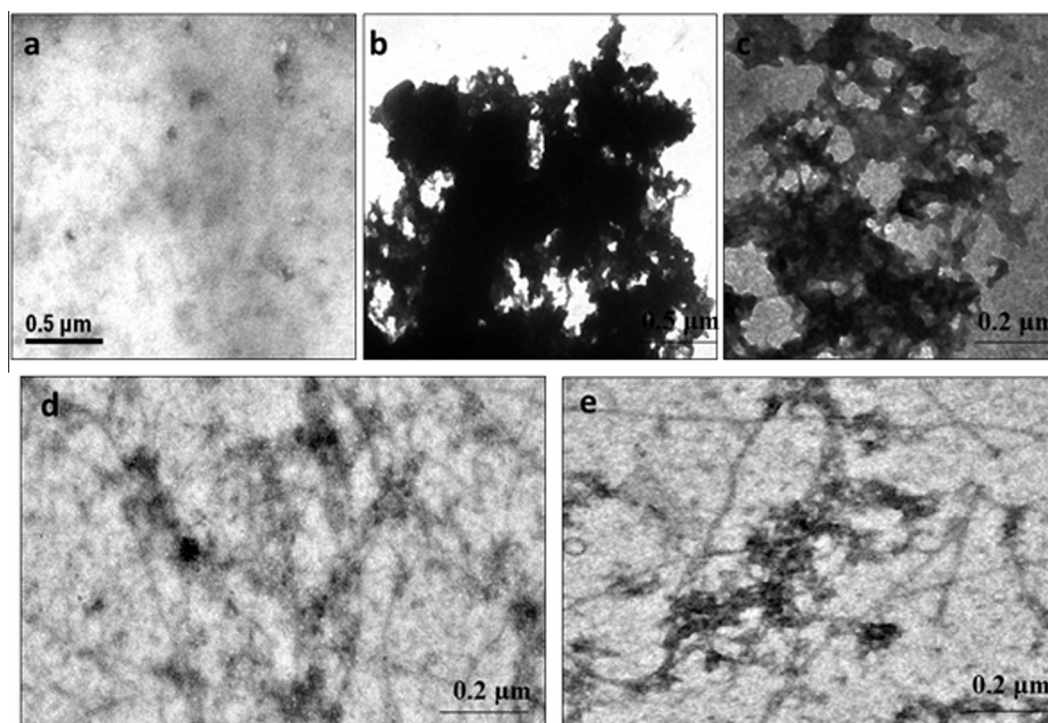


Figure 4. TEM images for A β -induced aggregation and test compound induced A β disaggregation. The incubations were carried out with following reagents: (a) 50 μ M A β_{1-42} alone at 0 h (b) 50 μ M A β_{1-42} alone at 48 h, 37 °C (c) 50 μ M A β_{1-42} and 25 μ M curcumin at 48 h, 37 °C (d) 50 μ M A β_{1-42} and 25 μ M compound **4d** at 48 h, 37 °C (e) 50 μ M A β_{1-42} and 25 μ M compound **4h** at 48 h, 37 °C.

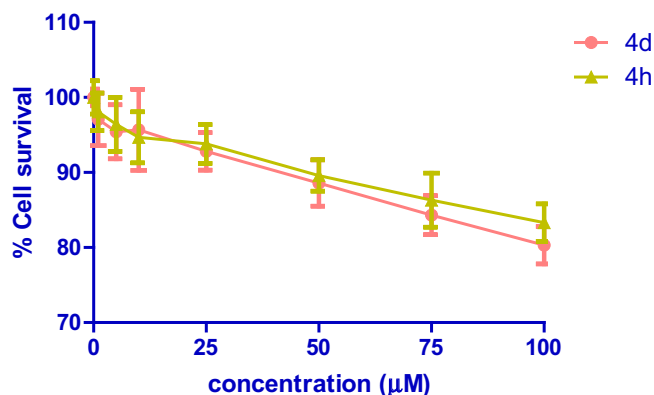


Figure 5. Effect of compounds **4d** and **4h** on the viability of SH-SY5Y cells. The cells were incubated with the indicated concentrations of the tested compounds for 48 h. The cell viability was assessed by MTT assay. Percentages of the cell viability are presented as mean \pm SEM from 3 independent experiments.

48 h, A β_{1-42} alone aggregated into mature, denser and bulky aggregates as compared to A β_{1-42} alone (Fig. 4a) kept at 0 °C. However, disaggregation effects were clearly visible upon addition of compounds **4d** and **4h** (25 μ M each), as fewer and slender A β fibrils were observed (Fig. 4d and e), respectively, as compared to A β_{1-42} alone (Fig. 4b) and standard curcumin (Fig. 4c). The results of TEM are consistent with ThT binding assay results which suggested that compounds **4d** and **4h** could inhibit A β aggregation noticeably through direct interaction with A β or by blocking PAS site of AChE.

2.3.6. Cytotoxicity of synthetic compounds in SH-SY5Y cells and neuroprotective effect on H₂O₂-induced oxidative cell damage in SH-SY5Y cells

To determine the potential cytotoxic effects of triazine derivatives on neuronal cell line SH-SY5Y, two most potent compounds **4d** and **4h** were selected for treatment, with different concentrations ranging from 1 to 100 μ M. After exposing the cells to these compounds for 48 h, the cell viability was evaluated by 3-(4,5-dimethylthiazol-2-yl)-2,5-diphenyltetrazolium (MTT) assay.^{36,37} The Figure 5 shows a dose-dependent effect of tested compounds on the viability of SH-SY5Y cells, for instance, **4d** (1 μ M: 97.1 \pm 3.5%; 5 μ M: 95.4 \pm 3.6%; 10 μ M: 95.7 \pm 5.4%; 25 μ M: 92.8 \pm 2.5%; 50 μ M: 88.6 \pm 3.1%; 75 μ M: 84.3 \pm 2.6% and 100 μ M: 80.3 \pm 2.5%) and **4h** (1 μ M: 98.1 \pm 2.5%; 5 μ M: 96.4 \pm 3.6%; 10 μ M: 94.7 \pm 3.4%; 25 μ M: 93.8 \pm 2.5%; 50 μ M: 89.6 \pm 2.1%; 75 μ M: 86.3 \pm 3.6% and 100 μ M: 83.3 \pm 2.5%), respectively. The results demonstrated that new compounds did not exhibit cytotoxic effect on the cells in the range of concentrations, which also covers the highest concentration (25 μ M) used in the experiment.

Oxidative stress plays an important role in neuronal degeneration. Oxidative damage marked by lipid peroxidation, nitration, reactive carbonyls, and nucleic acid oxidation is increased in vulnerable neurons in AD.¹⁵ Hence, the intracellular antioxidant activity of selected compounds **4d** and **4h** (5, 10 and 20 μ M) against H₂O₂-induced ROS in SH-SY5Y cells were assessed by DCFH-DA fluorescent assay. As illustrated in Figure 6, exposure of SH-SY5Y cells to H₂O₂ (200 μ M) for 24 h, increased the intracellular ROS accumulation by about 1.58 folds, p < 0.001. Treatment with compounds **4d** and **4h**, produced a moderate effect at lower doses 10 μ M, p < 0.05 while their protective ability against H₂O₂-induced ROS formation significantly improved at 20 μ M (p < 0.01) without affecting basal levels of ROS.

Furthermore, microscopic observations showed that a large number of H₂O₂-treated cells became rounded, vacuolated and floated which clearly indicated apoptosis or necrosis in these cells. All these morphological alterations clearly indicated H₂O₂ induced

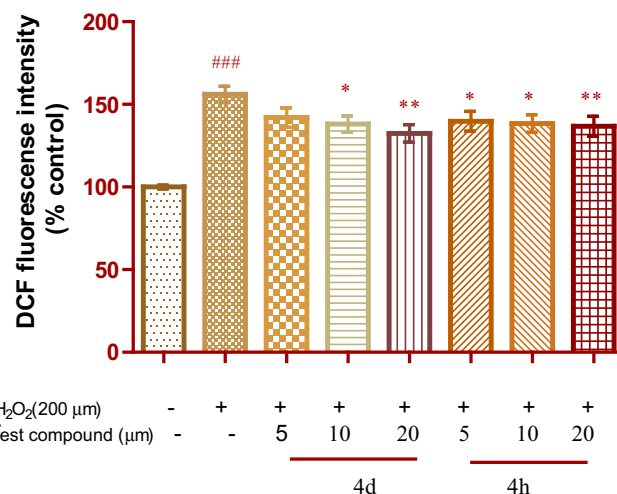


Figure 6. Neuroprotection against H₂O₂ toxicity in SH-SY5Y cells. Compounds **4d** and **4h** were tested for neuroprotective activity against H₂O₂ toxicity in neuroblastoma cell cultures. Results are expressed as percent viability compared to untreated control cells. All data were expressed as mean \pm SD of three experiments and each included triplicate sets. * p < 0.05, ** p < 0.01, *** p < 0.001 versus control; * p < 0.05, ** p < 0.01, *** p < 0.001 versus H₂O₂ alone. Statistical analysis was performed using one way ANOVA followed by Bonferroni test.

neurotoxicity in SH-SY5Y cells. However, compounds treatment (20 μ M) blocked these morphological changes and significantly prevented the cell death induced by H₂O₂ toxicity in these cells (Fig. 7c and d). These results indicate that the neuroprotective action of our synthesized compounds might come from radical scavenging action.

2.3.7. Neuroprotection against A β_{1-42} -induced toxicity

A β -induced apoptotic neuronal cell death is a critical event in the pathology of AD. The toxicity caused by A β_{42} is complex, which includes the generation of abnormally high concentration of reactive oxygen species, activating the release of damaging cytokines (e.g., interleukin-1, interleukin-6, TNF- α), and causing mitochondrial dysfunctions.³⁸ A separate set of experiments were conducted to assess the neurotoxic concentration of A β_{1-42} in SH-SY5Y neuroblastoma cells, using cell viability assay (Fig. 8). The neuroprotective potential of compounds of the representative compounds **4d** and **4h** on A β_{1-42} induced neurotoxicity were evaluated at three different concentrations, i.e., 5, 10 and 20 μ M. Treatment of cells with A β_{1-42} (25 μ M) for 48 h, resulted in marked decrease in cell viability (47.2%, p < 0.001) as compared to untreated control. The co-treatment of cells with compounds ameliorated A β_{1-42} induced neurotoxicity. As can be seen in Figure 8, the selected compounds exhibited neuroprotective effects at concentrations ranging from 5 to 20 μ M, with both compounds showing the highest protective capability.

Compound **4h** exhibited a significant effect in a dose dependant manner, i.e., 5 μ M, p < 0.05; 10 μ M p < 0.01 and 20 μ M, p < 0.001. While **4d** showed weaker effect at lower concentration however, displayed similar neuroprotective potential at the higher dose concentration of 10 μ M (p < 0.01) and 20 μ M (p < 0.001) as observed in compound **4h**.

Furthermore, microscopic observation revealed a marked change in the morphology of A β_{1-42} treated cells as compared to control cells (Fig. 9b). After A β_{1-42} treatment, cell loss with visibly shrink cell body, fading synapses, loss of adherence and fragmented or rounded floating cells which signifies onset of apoptosis or necrosis. However, compounds treatment significantly restored these alterations in SH-SY5Y cells (Fig. 9c and d). These results suggested that these novel compounds exerted

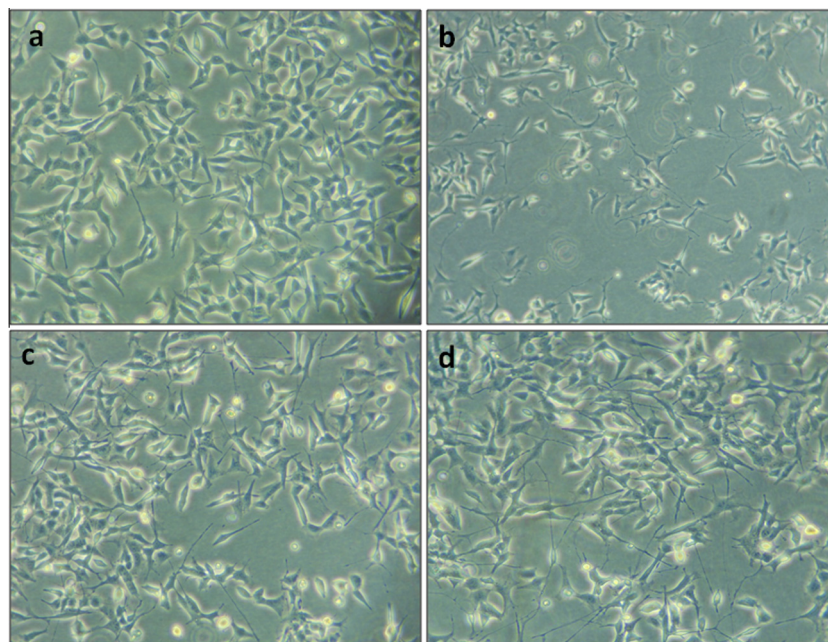


Figure 7. Phase-contrast micrographs showing H_2O_2 -induced neurotoxicity and neuroprotection of **4d** and **4h** in SH-SY5Y cells. (a) Cells without treatment showed healthy shapes. (b) H_2O_2 alone (200 μM) induced neurotoxicity. (c) Compound **4d** (20 μM) was given for 24 h with H_2O_2 (200 μM) at 37 $^\circ\text{C}$. (d) Compound **4h** (20 μM) was given for 24 h with H_2O_2 (200 μM) at 37 $^\circ\text{C}$ and co-treatment showed neuroprotection.

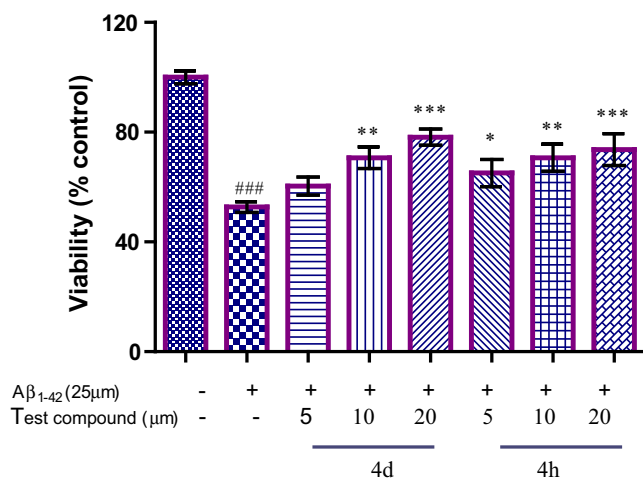


Figure 8. Neuroprotection against $\text{A}\beta$ -induced toxicity. Compounds **4d** and **4h** were tested for neuroprotective activity against $\text{A}\beta$ toxicity in SH-SY5Y neuroblastoma cell cultures. Results are expressed as percent viability compared to untreated control. All data were expressed as mean \pm SD of three experiments and each included triplicate sets. # $p < 0.05$, ## $p < 0.01$, ### $p < 0.001$ versus control; * $p < 0.05$, ** $p < 0.01$, *** $p < 0.001$ versus $\text{A}\beta_{1-42}$ alone. Statistical analysis was performed using one way ANOVA followed by Bonferroni test.

marked neuroprotection against $\text{A}\beta$ -induced neurotoxicity. Thus, the protective action against the $\text{A}\beta_{1-42}$ peptide of our synthetic compounds might be enhanced by the anti- $\text{A}\beta$ aggregation action.

2.4. Pharmacokinetic properties and drug likeness of compounds 4a–4h

A drug candidate should have desirable biopharmaceutical properties such as good solubility and good permeability, as well as optimal ADME properties. Hence, physicochemical indicators based on in silico models derived from in vitro and in vivo data, are increasingly used during the early stages of drug discovery to provide a comprehensive understanding of the key properties that

affect biological functions (ADME). In the present study, to predict the drug-likeness of the targeted compounds, about 45 physically significant descriptors and pharmacologically relevant properties of these compounds were calculated using QikProp module of the Schrödinger program.³⁹ A few significant indicators of their pharmacokinetic profiles were considered and are reported in Table 4. Fundamental physiochemical features of CNS active drugs are mainly related to their ability to penetrate the blood–brain barrier (BBB) and exhibit CNS activity. Our results indicated that compounds showed drug like characteristics based on Lipinski's rule of five (mol_MW < 500, QPlogPo/w < 5, donorHB \leq 5, acptHB \leq 10). Based on the predicted values for QPlogBB, QPlog Po/W and CNS activity, all compounds might be able to penetrate into the CNS. PSA is another important predictor for BBB. The calculated theoretical PSA values for all compounds may support their ability to penetrate the blood–brain barrier. Among calculated parameters, QPPCaco, QPlogBB, QPlogKh_{sa}, and QPPMDCK mainly account for the ability of the compound's distribution across BBB (QPPMDCK) and gut-blood barrier (QPPCaco). The amount of protein binding of CNS drugs is an important consideration which tends to be rather high. The predicted values of QPlogKh_{sa} for all compounds indicate their strong binding with plasma protein. In addition, the results showed that all compounds displayed excellent oral absorption. The predicted ADME properties revealed that all compounds possess appropriate pharmacokinetic profiles required to penetrate BBB and therefore, could be considered as good candidate for drug development.

3. Conclusion

In summary, eight new triazine derivatives were synthesized and characterized as multifunctional anti-Alzheimer agents. All of these synthetic compounds showed potent AChE inhibitory activity and good selectivity for AChE over BuChE. Our synthetic derivatives also exhibited potent radical scavenging activity. Compounds **4d** and **4h** exhibited highest anti- $\text{A}\beta_{1-42}$ aggregation potency with IC_{50} values of 10.1 and 10.9 μM , respectively. In addition, TEM studies have also confirmed the anti- $\text{A}\beta_{1-42}$ aggregation property

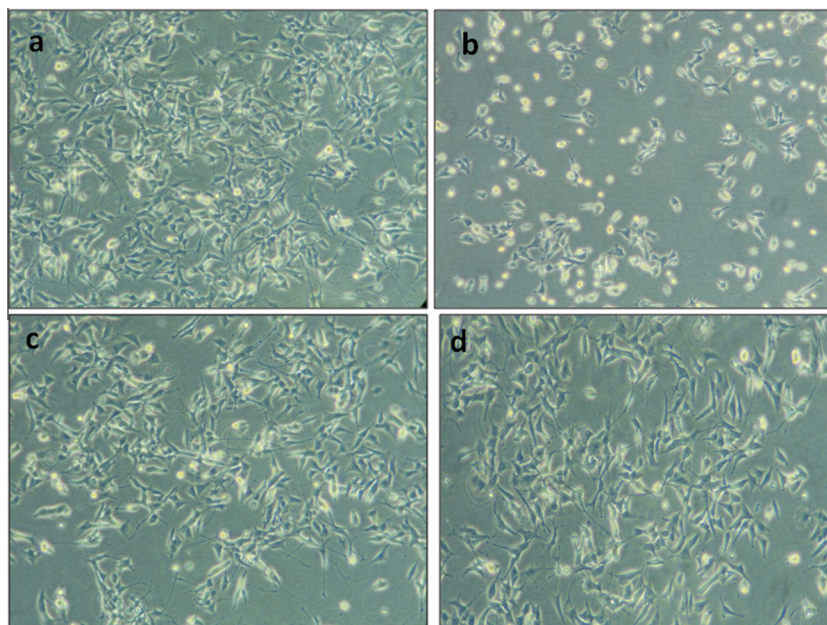


Figure 9. Phase-contrast micrographs showing A β -induced neurotoxicity and neuroprotection of **4d** and **4h** in SH-SY5Y cells. (a) Cells without treatment showed healthy shapes. (b) A β alone (25 μ M) induced neurotoxicity. (c) Compound **4d** (20 μ M) was given for 24 h with A β (25 μ M) at 37 $^{\circ}$ C. (d) Compound **4h** (20 μ M) was given for 24 h with A β (25 μ M) at 37 $^{\circ}$ C.

Table 4
Predicted ADMET properties of the target compounds **4a–4h**

Compound	Mol_MW (130–725)	HB donors (0–6)	HB acceptors (2–20)	QPlog Po/W (–2 to 6.5)	Rotatable bonds (0–15)	PSA (7–200)	SASA (300–1000)	CNS (–2 to 2)	QPPcaco (<25 poor, >500 great)	QPlogBB (–3 to 1.2)	QPPMDCK (<25 poor, >500 great)	QPlog KhSa (–1.5 to 1.5)	% human oral absorption (>80% high, <25% poor)
4a	481.482	2	7.5	5.076	5	91.668	822.889	–1	820.768	–0.794	1759.931	0.792	95.867
4b	531.542	2	7.5	6.155	5	89.742	894.235	–1	889.014	–0.806	1918.451	1.16	89.849
4c	553.496	2	7.5	6.259	5	89.65	877.029	0	890.058	–0.594	5182.969	1.082	90.468
4d	569.951	2	7.5	6.539	5	89.734	893.439	0	888.832	–0.535	7667.097	1.156	92.094
4e	535.506	2	7.5	6.085	5	89.745	871.157	0	889.652	–0.669	3475.774	1.047	89.441
4f	497.534	2	8.25	5.189	6	97.542	853.357	–1	935.115	–0.979	775.624	0.797	100
4g	515.979	2	7.5	5.861	5	89.742	872.936	–1	888.284	–0.806	1739.827	1.056	88.121
4h	547.541	2	8.25	5.937	6	98.033	898.928	–1	888.48	–0.863	1917.601	1.009	88.565

MW: molecular weight, HBA: hydrogen-bond acceptor atoms, HBD: hydrogen-bond donor atoms, PSA: polar surface area, SASA: total solvent accessible surface area, QPlogPo/w: Predicted octanol/water partition coefficient, CNS: Predicted central nervous system activity, QPPcaco: Caco-2 cell permeability in nm/sec, QPPMDCK: Predicted apparent MDCK cell permeability in nm/sec, QPlogBB: brain/blood partition coefficient, QPlogKhSa: binding to human serum albumin, Percent Human-oral Absorption: human oral absorption on 0–100% scale.

of compounds **4d** and **4h**. The molecular modelling studies indicated that our synthetic derivatives have significant binding affinity with both CAS and PAS of the AChE. In addition, our synthetic compounds showed a neuroprotective effect against both oxidative stress induced by H₂O₂ and A β _{1–42} toxicity. Taken together, the data show that triazine derivatives can be considered very promising lead compounds for treatment of AD.

4. Experimental

4.1. Chemistry

All reagents and solvents were commercially available and used as purchased without further purification. Melting points (mp) were determined on a Stuart Scientific SMP1 apparatus and are uncorrected. Proton nuclear magnetic resonance (¹H NMR) spectra were recorded on a Bruker 400 MHz FT spectrometer. Proton chemical shifts are reported in ppm (TMS, δ 0.00) or with the solvent reference relative to TMS employed as the internal standard (CDCl₃, δ 7.26; DMSO-*d*₆ δ 2.54) and multiplicities of NMR signals are design-

nated as s (singlet), d (doublet), dd (double doublet), t (triplet), q (quartet), br (broad), m (multiplet, for unresolved lines). LCMS of the compounds were carried out on applied biosystem (abscix 2000 triple quad). Column chromatography was performed on columns packed with alumina from Merck (70–230 mesh). Aluminum oxide thin-layer chromatography (TLC) cards from Merck (aluminum oxide-precoated aluminum cards with fluorescent indicator detectable at 254 nm) were used for TLC. Developed plates were visualized by a Spectroline ENF 260C/FE UV apparatus. Organic solutions were dried over anhydrous sodium sulfate. Evaporation of the solvents was carried out on a Büchi rotavapor R-100 equipped with a Büchi V-100 vacuum controller. Elemental analyses were obtained in an Elementar Vario analyser. Elemental analyses of the compounds were found to be within \pm 0.4% of the theoretical values. The purity of tested compounds was >95%.

4.1.1. General procedure for the synthesis of mono-substituted triazine (2a–2h)²²

The synthesis of mono-substituted triazine is depicted in Scheme 1. 2,4,6-trichloro-1,3,5-triazine (5.03 g; 1.1 equiv) was

dissolved in anhydrous THF at -10°C and K_2CO_3 (3.43 g; 1 equiv) was added. Appropriate aromatic amines (4 g; 1 equiv) were dissolved in THF and were added drop wise to the reaction mixture for half an hour with constant stirring. The progress of the reaction was monitored by thin layer chromatography. After the completion of the reaction, the reaction mixture was dried with a rotatory evaporator. The reaction was quenched with water and extracted with ethylacetate (2×50 ml). The organic phase was washed with brine solution, dried over Na_2SO_4 and evaporated at reduced pressure to get the crude products. The crude products were purified by silica gel column chromatography eluted with petroleum ether and EtOAc (2–3%) to give the pure compounds **2a–2h**, which were used for the next step reaction.

4.1.2. General procedure for the synthesis of di-substituted triazine (**3a–3h**)²²

A solution of appropriate aromatic amine (0.87 g; 1 equiv) in THF (5 ml) was added drop wise to the stirred solution of mono-substituted triazine (2.5 g; 1 equiv) and K_2CO_3 (1.1 g; 1 equiv) in anhydrous DMF (5 ml) at 0°C . Then the reaction mixture was continued to stir at room temperature for 6–12 h. The progress of the reaction was monitored by thin layer chromatography. After the completion of the reaction, the reaction mixture was quenched with water and extracted with ethylacetate (3×50 ml). The organic phase was washed with brine solution and then dried over Na_2SO_4 and evaporated to dryness. The compounds **3a–3h** were also purified by column chromatography eluted with petroleum ether and EtOAc (6–8%) and were used for the final step.

4.1.3. General procedure for the synthesis of tri-substituted triazine (**4a–4h**)

2-(Piperazin-1-yl)nicotinonitrile (**6**) was synthesized while reacting 2-chloronicotinonitrile with piperazine in presence of base as K_2CO_3 .²³ 0.56 g (1.2 equiv) of (**6**) was dissolved in 1,4-dioxane and K_2CO_3 (0.38 g; 1.1 equiv) was added at room temperature. Di-substituted triazine compounds (**3a–3h**) (1 g; 1 equiv) dissolved in 1,4-dioxane were added drop wise for 30 minutes at room temperature. After the addition, the reaction mixtures were heated under reflux for 12–16 h. The progress of the reactions were monitored by thin layer chromatography. After the completion of the reaction, the reaction mixtures were filtered and the residues were washed with 1,4-dioxane. The filtrates obtained were vacuum dried. The crude tri-substituted compounds obtained were purified using column chromatography eluted with petroleum ether and EtOAc (60–70%) to give the pure compounds **4a–4h**.

2,4,6-Trichloro-1,3,5-triazine undergoes temperature dependent nucleophilic aromatic substitution reaction in which all the three chlorine atoms were substituted step by step with different nucleophiles. The first two steps, occurred below -10°C with 1 equiv of base (K_2CO_3) and at room temperature with 1–1.2 equiv K_2CO_3 , respectively. Third substitution occurred at 110°C in presence of base K_2CO_3 and 1,4-dioxane. All the synthesized compounds were purified by column chromatography using EtOAc/Pet. ether as eluent and characterized by various spectroscopic techniques.

4.1.4. Synthesis of 2-(4-(4-(cyclopropylamino)-6-(3-(trifluoromethyl)phenylamino)-1,3,5-triazin-2-yl)piperazin-1-yl)nicotinonitrile (**4a**)

Sticky semisolid which later on solidified, light brownish, ($R_f = 0.2$ in ethylacetate), yield = 72%, mp $165\text{--}167^{\circ}\text{C}$, ^1H NMR (300 MHz, CDCl_3) δ 8.37 (s, 2H), 8.07 (s, 1H), 7.79 (d, $J = 7.2$ Hz, 1H), 7.50 (d, $J = 6.9$ Hz, 1H), 7.33 (1H), 6.79 (d, $J = 4.8$ Hz, 1H), 5.69 (s, 1H), 3.97 (8H), 2.80 (s, 1H), 2.05 (s, 1H), 1.26 (s, 1H), 0.80 (s, 2H), 0.54 (s, 1H). ^{13}C NMR (75 MHz, CDCl_3) δ 171.19, 160.63, 151.87, 143.85, 140.24, 129.04, 122.18, 118.58, 117.98, 116.54,

114.39, 95.11, 72.74, 60.41, 47.86, 43.03, 23.42, 21.02, 14.17, 7.12. LCMS: (ESI, m/z): $[\text{M}+\text{H}]^+$ Calcd for $\text{C}_{23}\text{H}_{22}\text{F}_3\text{N}_9$ 481.9, found: 482.1. Elemental Anal.: Calcd C, 57.37; H, 4.61; N, 26.18, found C, 57.49; H, 4.80; N, 26.07.

4.1.5. Synthesis of 2-(4-(4-(*p*-toluidino)-6-(3-(trifluoromethyl)phenylamino)-1,3,5-triazin-2-yl)piperazin-1-yl)nicotinonitrile (**4b**)

Solid, off white, ($R_f = 0.2$ in ethylacetate), yield = 76%, mp $178\text{--}180^{\circ}\text{C}$, ^1H NMR (300 MHz, CDCl_3) δ 8.37 (dd, $J = 4.8, 1.8$ Hz, 1H), 8.06 (s, 1H), 7.80 (dd, $J = 7.8, 2.1$ Hz, 1H), 7.54 (d, $J = 8.1$ Hz, 1H), 7.41 (d, $J = 8.4$ Hz, 3H), 7.33 (s, 1H), 7.27 (s, 1H), 7.13 (d, $J = 8.1$ Hz, 3H), 6.80 (1H), 3.99 (4H), 3.79 (4H), 2.32 (s, 3H). ^{13}C NMR (75 MHz, CDCl_3) δ 165.12, 164.38, 164.21, 160.65, 151.90, 143.87, 139.66, 135.98, 132.96, 131.32, 129.40, 125.91, 122.69, 120.76, 119.09, 117.97, 116.81, 114.46, 95.21, 47.87, 43.20, 29.69, 20.80. LCMS: (ESI, m/z): $[\text{M}+\text{H}]^+$ Calcd for $\text{C}_{27}\text{H}_{24}\text{F}_3\text{N}_9$ 531.2, found: 532.2. Elemental Anal.: Calcd C, 61.01; H, 4.55; N, 23.72, found C, 61.23; H, 4.69; N, 23.62.

4.1.6. Synthesis of 2-(4-(4-(2,4-difluorophenylamino)-6-(3-(trifluoromethyl)phenylamino)-1,3,5-triazin-2-yl)piperazin-1-yl)nicotinonitrile (**4c**)

Solid, white, ($R_f = 0.2$ in ethylacetate), yield = 69%, mp $170\text{--}172^{\circ}\text{C}$, ^1H NMR (300 MHz, CDCl_3) δ 8.38 (d, $J = 4.8$ Hz, 1H), 8.17 (d, $J = 6.3$ Hz, 1H), 8.07 (s, 1H), 7.82 (d, $J = 7.5$ Hz, 1H), 7.56 (d, $J = 7.2$ Hz, 1H), 7.42 (d, $J = 7.8$ Hz, 1H), 7.28 (d, $J = 12.6$ Hz, 2H), 7.19 (s, 1H), 6.90 (dd, $J = 2.1, 10.8$ Hz, 2H), 6.82 (dd, $J = 7.8, 5.1$ Hz, 1H), 4.00 (s, 4H), 3.79 (s, 4H). ^{13}C NMR (75 MHz, CDCl_3) δ 165.05, 164.42, 163.58, 160.68, 151.91, 143.87, 139.43, 136.83, 131.39, 129.27, 127.45, 123.46, 122.79, 119.39, 117.93, 116.86, 114.58, 111.03, 110.72, 108.46, 103.63, 101.74, 95.32, 47.87, 43.19. LCMS: (ESI, m/z): $[\text{M}+\text{H}]^+$ Calcd for $\text{C}_{26}\text{H}_{20}\text{F}_5\text{N}_9$ 553.1, found: 554.2. Elemental Anal.: Calcd C, 56.42; H, 3.64; N, 22.78, found C, 56.54; H, 3.73; N, 22.56.

4.1.7. Synthesis of 2-(4-(4-(3-chloro-4-fluorophenylamino)-6-(3-(trifluoromethyl)phenylamino)-1,3,5-triazin-2-yl)piperazin-1-yl)nicotinonitrile (**4d**)

Solid, white, ($R_f = 0.3$ in ethylacetate), yield = 75%, mp $175\text{--}177^{\circ}\text{C}$, ^1H NMR (300 MHz, CDCl_3) δ 8.39 (d, $J = 4.8$ Hz, 1H), 8.03 (s, 1H), 7.82 (dd, $J = 7.8, 2.1$ Hz, 1H), 7.76 (d, $J = 9.0$ Hz, 1H), 7.60 (d, $J = 7.8$ Hz, 1H), 7.44 (d, $J = 7.8$ Hz, 2H), 7.30 (d, $J = 6.9$ Hz, 3H), 7.09 (d, $J = 8.7$ Hz, 1H), 6.82 (dd, $J = 7.5, 4.8$ Hz, 1H), 4.00 (t, $J = 4.5, 4\text{H}$), 3.79 (t, $J = 5.7, 4\text{H}$). ^{13}C NMR (75 MHz, CDCl_3) δ 164.84, 163.73, 160.67, 151.90, 143.85, 139.25, 135.26, 130.95, 129.33, 123.00, 122.64, 120.68, 120.06, 119.97, 119.58, 119.53, 117.88, 117.01, 116.59, 116.29, 114.64, 95.39, 47.83, 43.28. LCMS: (ESI, m/z): $[\text{M}+\text{H}]^+$ Calcd for $\text{C}_{26}\text{H}_{20}\text{ClF}_4\text{N}_9$ 569.1, found: 570.3. Elemental Anal.: Calcd C, 54.79; H, 3.54; N, 22.12, found C, 56.94; H, 3.70; N, 22.03.

4.1.8. Synthesis of 2-(4-(4-(4-fluorophenylamino)-6-(3-(trifluoromethyl)phenylamino)-1,3,5-triazin-2-yl)piperazin-1-yl)nicotinonitrile (**4e**)

Solid, snow white, ($R_f = 0.3$ in ethylacetate), yield = 77%, mp $139\text{--}142^{\circ}\text{C}$, ^1H NMR (300 MHz, DMSO) δ 9.60 (s, 1H), 9.35 (s, 1H), 8.44 (dd, $J = 4.8, 1.8$ Hz, 1H), 8.24 (s, 1H), 8.12 (d, $J = 7.5$ Hz, 1H), 7.98 (s, 1H), 7.74 (s, 2H), 7.52 (s, 1H), 7.29 (d, $J = 7.8$ Hz, 1H), 7.13 (s, 2H), 6.96 (dd, $J = 7.5, 4.8$ Hz, 1H), 3.94 (s, 4H), 3.74 (s, 4H). ^{13}C NMR (75 MHz, DMSO) δ 164.53, 164.03, 160.14, 159.09, 155.93, 152.05, 144.36, 140.94, 136.18, 129.53, 129.00, 126.10, 123.20, 121.94, 117.85, 115.89, 115.05, 114.86, 114.76, 94.43, 47.43, 42.59. LCMS: (ESI, m/z): $[\text{M}+\text{H}]^+$ Calcd for $\text{C}_{26}\text{H}_{21}\text{F}_4\text{N}_9$

535.1, found: 536.2. Elemental Anal.: Calcd C, 58.32; H, 3.95; N, 23.54, found C, 58.56; H, 3.99; N, 23.33.

4.1.9. Synthesis of 2-(4-(4-(2-fluorophenylamino)-6-(4-methoxyphenylamino)-1,3,5-triazin-2-yl)piperazin-1-yl)nicotinonitrile (4f)

Solid, off white, (R_f = 0.2 in ethylacetate), yield = 70%, mp 185–187 °C, ^1H NMR (300 MHz, CDCl_3) δ 8.37 (dd, J = 4.5, 1.8 Hz, 1H), 8.31 (d, J = 8.1 Hz, 1H), 7.81 (dd, J = 7.5, 1.8 Hz, 1H), 7.46 (d, J = 8.7 Hz, 2H), 7.26 (s, 2H), 7.11 (d, J = 8.1 Hz, 3H), 6.90 (d, J = 9.0 Hz, 2H), 6.80 (dd, J = 7.8, 4.8 Hz, 1H), 3.99 (s, 3H), 3.82 (8H). ^{13}C NMR (75 MHz, CDCl_3) δ 165.05, 160.65, 155.94, 151.91, 143.89, 131.64, 124.13, 124.08, 122.96, 122.85, 122.61, 122.08, 118.00, 115.00, 114.74, 114.45, 114.06, 110.14, 95.18, 55.54, 47.90, 43.20. LCMS: (ESI, m/z): $[\text{M}+\text{H}]^+$ Calcd for $\text{C}_{26}\text{H}_{24}\text{FN}_9\text{O}$ 497.2, found: 498.1. Elemental Anal.: Calcd C, 62.77; H, 4.86; N, 25.34, found C, 62.90; H, 4.97; N, 25.19.

4.1.10. Synthesis of 2-(4-(4-(*p*-toluidino)-6-(3-chloro-4-fluorophenylamino)-1,3,5-triazin-2-yl)piperazin-1-yl)nicotinonitrile (4g)

Solid, off white, (R_f = 0.2 in ethylacetate), yield = 77%, mp 195–197 °C ^1H NMR (300 MHz, CDCl_3) δ 8.37 (d, J = 4.8 Hz, 1H), 7.82 (d, J = 7.8 Hz, 2H), 7.41 (d, J = 8.1 Hz, 2H), 7.26 (s, 2H), 7.15 (d, J = 8.7 Hz, 2H), 7.07 (d, J = 8.7 Hz, 1H), 7.03 (s, 1H), 6.80 (dd, J = 7.8, 4.8 Hz, 1H), 3.98 (t, J = 4.2 Hz, 4H), 3.79 (t, J = 3 Hz, 4H), 2.33 (s, 3H). ^{13}C NMR (75 MHz, CDCl_3) δ 165.07, 164.10, 160.65, 155.54, 151.91, 143.89, 135.96, 135.70, 132.96, 129.43, 122.25, 120.74, 119.48, 117.98, 116.46, 116.17, 114.48, 95.22, 47.89, 43.15, 29.70, 20.84. LCMS: (ESI, m/z): $[\text{M}+\text{H}]^+$ Calcd for $\text{C}_{26}\text{H}_{23}\text{ClFN}_9$ 515.1, found: 516.0. Elemental Anal.: Calcd C, 60.52; H, 4.49; N, 24.43, found C, 60.69; H, 4.58; N, 24.35.

4.1.11. Synthesis of 2-(4-(4-(4-methoxyphenylamino)-6-(3-(trifluoromethyl)phenylamino)-1,3,5-triazin-2-yl)piperazin-1-yl)nicotinonitrile (4h)

Solid, snow white, (R_f = 0.3 in ethylacetate), yield = 68%, mp 179–180 °C ^1H NMR (300 MHz, CDCl_3) δ 8.37 (d, J = 2.4 Hz, 1H), 8.08 (s, 1H), 7.80 (d, J = 7.5 Hz, 1H), 7.55 (d, J = 7.8 Hz, 1H), 7.42 (d, J = 8.7 Hz, 3H), 7.26 (s, 1H), 7.15 (s, 1H), 6.89 (d, J = 8.7 Hz, 3H), 6.80 (s, 1H), 3.99 (s, 3H), 3.81 (8H). ^{13}C NMR (75 MHz, CDCl_3) δ 165.13, 164.53, 164.24, 160.67, 156.00, 151.90, 143.88, 139.68, 131.56, 131.32, 130.90, 122.61, 119.10, 117.98, 116.69, 114.46, 114.12, 95.21, 95.04, 55.51, 47.89, 47.70, 43.16. LCMS: (ESI, m/z): $[\text{M}+\text{H}]^+$ Calcd for $\text{C}_{27}\text{H}_{24}\text{F}_3\text{N}_9\text{O}$ 547.2, found: 548.2. Elemental Anal.: Calcd C, 59.23; H, 4.42; N, 23.02, found C, 59.46; H, 4.60; N, 22.89.

4.2. Docking protocol

Molecular docking and Scoring of ligands with AChE and BuChE were carried out using Pardock module of *Sanjeevini*^{25,26} a comprehensive drug design suite, based on physicochemical descriptors. It integrates several protocols and handles protein and ligands at atomic level where the hydrogen added protein is prepared in a force field compatible manner. Ligand was considered in its input pose for the calculation. Addition of hydrogen to the ligand was achieved utilizing xleap of AMBER⁴⁰ and geometry optimization and partial charge calculations were performed using AM1-BCC procedure.

The docked structures are energy minimized using the sander module of AMBER and scored using scoring function *Bapp*⁴¹ which is an all atom based scoring function, constituting electrostatics, van der Waals, hydrophobicity, loss of conformational entropy of protein side chains after complexation. Docked structures were visualized using *Chimera*.⁴²

4.3. Biological assays

4.3.1. Inhibition of AChE and BuChE

AChE and BuChE inhibitory activities of the test compounds were determined by the modified Ellman's method. Briefly, Stock solutions of tested compounds (10 mM) were prepared in ethanol and diluted using 0.1 M $\text{KH}_2\text{PO}_4/\text{K}_2\text{HPO}_4$ buffer (pH 8.0) to afford a final concentration range between (0.01–100) μM . Enzyme solutions were prepared by dissolving lyophilized powder in double-distilled water. The assay solution consisted of 1 mL of 0.1 M phosphate buffer $\text{KH}_2\text{PO}_4/\text{K}_2\text{HPO}_4$, 25 μL of AChE (0.22 U/mL, E.C. 3.1.1.7, from electric eel) or 25 μL of BuChE (0.06 U/mL, E.C. 3.1.1.8, from equine serum) and 100 μL of various concentrations of test compounds which was allowed to stand for 5 min before 100 μL of 0.01 M DTNB were added. A positive control of donepezil was used in the same range of concentrations. The reaction was started by addition of 20 μL of the 0.075 M substrate solution (acetylthiocholine/butyrylthiocholine) and exactly 2 min after substrate addition the absorption was measured at 25 °C at 412 nm. The non-enzymatic hydrolysis of acetylthiocholine/butyrylthiocholine iodide was also measured in enzyme-free assay systems, and the results were employed as blank. In control experiments, inhibitor-free assay systems were utilized to measure the full activity. The percent inhibition was calculated by the following expression: $(1 - \text{Ai}/\text{Ac}) \times 100$, where Ai and Ac are the absorbances obtained for AChE in the presence and absence of the inhibitors, respectively, after subtracting the respective background. Each experiment was performed in triplicate, and the mean \pm standard deviation was calculated. Data from concentration-inhibition experiments of the inhibitors were calculated by nonlinear regression analysis, using the Graph Pad Prism 5 program.

4.3.2. Kinetic study of AChE

Kinetic study of AChE was performed using a reported method.⁴³ Test compound was added into the assay solution and pre-incubated with the enzyme at 37 °C for 15 min, followed by the addition of substrate. Kinetic characterization of the hydrolysis of ATC catalysed by AChE was carried out spectrometrically at 412 nm. A parallel control was made with the assay solution of no inhibitor for each times. The plots were assessed by a weighted least square analysis that assumed the variance of V to be a constant percentage of V for the entire data set. Slopes of these reciprocal plots were then plotted against the concentration of the inhibitors in a weighted analysis and K_i was determined as the ratio of the replot intercept to the replot slope.

4.3.3. Thioflavin T (ThT) assay

Commercially available peptides were first treated with hexafluoroisopropanol (HFIP) at 5 mg/ml to avoid self-aggregation. The clear solution containing the dissolved peptide was then aliquoted in micro centrifuge tube. The HFIP was allowed to evaporate under a stream of nitrogen until a clear film remained in the test tube. The pre-treated $\text{A}\beta_{1-42}$ samples were then dissolved in DMSO in order to have a stable stock solution ($\text{A}\beta$ = 1 mM). For the inhibition of self-mediated $\text{A}\beta_{1-42}$ aggregation experiment, the $\text{A}\beta$ stock solution was diluted with 50 mM phosphate buffer (pH 7.4) to 25 μM before use. A mixture of the peptide (10 μL , 25 μM , final concentration) with or without the tested compound (25 μM) was incubated at 37 °C for 48 h. To quantify amyloid fibril formation, the thioflavin-T fluorescence method was used. Blanks containing 50 mM phosphate buffer (pH 7.4) instead of $\text{A}\beta$ with or without inhibitors were also carried out. After incubation, samples were diluted to a final volume of 200 μL with 50 mM glycine-NaOH buffer (pH 8.0) containing thioflavin-T (5 μM). Then the fluorescence intensities were recorded five minutes later (excitation, 450 nm; emission, 485 nm). The percent inhibition of aggregation

was calculated by the expression $(1 - \text{Ifi/Ifc}) \times 100\%$ in which Ifi and Ifc are the fluorescence intensities obtained for A β in the presence and absence of inhibitors after subtracting the background, respectively. Each measurement was run in triplicate.

4.3.4. Oxygen radical absorbance capacity (ORAC-FL) assay

The reaction was carried out in 75 mM phosphate buffer (pH 7.4), and the final reaction mixture was 200 μL . Antioxidant (20 μL) and FL (120 μL ; 70 mM, final concentration) solutions were placed in a black 96-well microplate (96F untreat, Nunc). The mixture was preincubated for 15 min at 37 $^{\circ}\text{C}$, and then AAPH solution (60 μL , 12 mM, final concentration) was added rapidly using a multichannel pipette. The microplate was immediately placed in the reader and the fluorescence recorded every minute for 80 min (excitation, 485 nm; emission, 520 nm). Samples were measured at different concentrations (1–25 μM). A blank (FL+AAPH) using phosphate buffer instead of the tested compound and eight calibration solutions using Trolox (1–25 μM , final concentration) as antioxidant were also carried out in each assay. A blank using phosphate buffer instead of the tested compound was also carried out. All of the reaction mixtures were prepared in triplicate, and at least three independent runs were performed for each sample. The antioxidant curves (fluorescence vs time) were normalized to the curve of the blank. The area under the fluorescence decay curve (AUC) was calculated using the following equation:

$$\text{AUC} = 1 + \sum_{i=1}^{i=80} (f_i/f_0)$$

where f_0 is the initial fluorescence reading at 0 min and f_i is the fluorescence reading at time i . The net AUC was calculated by the following equation: $\text{AUC}_{\text{sample}} - \text{AUC}_{\text{blank}}$. The regression equations between the net AUC and the Trolox concentrations were calculated. The ORAC-FL value for each sample was calculated using the standard curve, and the ORAC-FL value of each tested compound is thus expressed as Trolox equivalents.

4.3.5. TEM assay

A β_{1-42} peptide (Sigma) stock was diluted with 20 mM phosphate buffer (pH 7.4) at 4 $^{\circ}\text{C}$ to 40 mM before use. For the inhibition of A β_{1-42} aggregation experiment, A β_{1-42} was incubated with in the presence and absence of compounds **4d**, **4h** and Curcumin at 37 $^{\circ}\text{C}$ for 48 h. The final concentration of A β_{1-42} and compounds were 50 μM and 25 μM , respectively. Aliquots (10 μL) of the samples were placed on a carbon coated copper/rhodium grid for 2 min at room temperature. Each grid was stained with uranyl acetate (1%) for 2 min. Excess staining solution was removed and the specimen was transferred for imaging with transmission electron microscopy (JEOL JEM-1400).

4.3.6. Cell toxicity assay

The toxicity effect of **4d** and **4h** on human neuroblastoma cells (SH-SY5Y) cells was examined according to the previous method.³⁷ The SH-SY5Y cells were cultured in Dulbecco's minimum essential medium (DMEM) supplemented with 10% fetal bovine serum (FBS), 1% penicillin–streptomycin solution (10,000 units of penicillin and 10 mg of streptomycin in 0.9% NaCl) at 37 $^{\circ}\text{C}$ in a humidified atmosphere containing 5% CO_2 . The cells were plated in 96-well plate at a density 2000 cells/well and cultured for 24 h. Next, cells were exposed to the tested compounds at different concentrations (0.1–100 μM) for 48 h. Stock solution of tested compound was prepared in DMSO and diluted in complete medium to give final concentrations. Cytotoxicity assay was performed after 48 h incubation with compounds in triplicates. The MTT reagent was added to each well for additional 4 h followed by solubilisation of formazan crystals in DMSO. The absorbance of each well was

measured using a microculture plate reader with a test wavelength of 570 nm and a reference wavelength of 630 nm. Results are expressed as the mean \pm SD of three independent experiments.

4.3.7. A β_{1-42} -induced cytotoxicity

A β_{1-42} peptides were first dissolved in hexafluoroisopropanol to 1 mg/ml, sonicated, incubated at room temperature for 24 h and lyophilized. The resulting A β_{1-42} peptide film was dissolved with dimethylsulfoxide and stored at -20°C until use. SH-SY5Y cells were harvested from flasks and plated in 96-well polystyrene plates with approximately 2×10^4 cells per well. Plates were incubated at 37 $^{\circ}\text{C}$ for 24 h to allow cells to attach. A β_{1-42} with or without compounds **4d** and **4h** were diluted with fresh medium and added to individual wells. The plates were then incubated for an additional 48 h at 37 $^{\circ}\text{C}$. Cell viability was determined using MTT assay and expressed as a percentage of control cells. Image micrographs were also taken with the help camera attached to the microscope (Olympus, Japan) to assess morphological alterations in SH-SY5Y cells after 48 h of treatment.

4.3.8. ROS measurements under H_2O_2 -induced cellular stress

ROS assay was performed in living cells as previously described by Wang and Zhu.⁴⁴ SH-SY5Y cells were seeded at 2×10^4 cells per well in 96-well plates for neuroprotection activity assay. Briefly, intracellular ROS production was measured from SH-SY5Y cells by treating them with fluorescent probe 2',7'-dichlorofluorescein diacetate (DCFH-DA) for 20 min after 24 h of H_2O_2 (200 μM) treatment in the presence or absence of compounds **4d** and **4h** (5, 10 and 20 μM). As a nonpolar compound, DCFH-DA crosses cell membrane and cellular esterases cleaved diacetate groups of DCFH-DA to form non-fluorescent 2',7'-dichlorofluorescein (DCFH). In the presence of intracellular ROS, DCFH is oxidized very quickly to highly fluorescent DCFH. The total fluorescence was measured using ELISA plate reader (Tecan infinity 20) at an emission wavelength of 488 nm and an excitation wavelength of 524 nm. Image micrographs were also taken with the help camera attached to the microscope (Olympus, Japan) to assess morphological alterations in SH-SY5Y cells after 24 h of treatment.

4.4. In silico ADME property prediction

ADME (absorption, distribution, metabolism and excretion) properties of compounds were predicted using QikProp program, v. 3.5 (Schrödinger, LLC, New York, USA).³⁹ This gave an estimate of the physicochemical properties and the bioavailability of the compounds. Parameters such as polar surface area (PSA), solvent accessible surface area (SASA), CNS activity (Predicted central nervous system activity, QPPCaco (Predicted apparent Caco-2 cell permeability in nm/s. Caco-2 cells is a model for the gut blood barrier), QPlogBB (Predicted brain/blood partition coefficient), QPPMDCK (Predicted apparent MDCK cell permeability in nm/s. MDCK cells are considered to be a good mimic for the blood–brain barrier), QPlogKhsa (Prediction of binding to human serum albumin) and percent human oral absorption (Predicted human oral absorption on 0–100% scale) were calculated. The acceptability of the compounds based on the Lipinski's rule of five were also estimated from the results.

Acknowledgements

M.M. is thankful to University Grants Commission (UGC), Government of India for financial assistance through Central University Ph.D. Students Fellowship. J.K. thanks to Council of Scientific and Industrial Research (CSIR) for financial assistance through SRF.

Supplementary data

Supplementary data (^1H NMR, ^{13}C NMR spectra and Mass Spectra of new compounds) associated with this article can be found, in the online version, at <http://dx.doi.org/10.1016/j.bmc.2016.04.041>. These data include MOL files and InChIKeys of the most important compounds described in this article.

References and notes

- Selkoe, D. J. *Ann. Intern. Med.* **2004**, *140*, 627.
- Salloway, S.; Correia, S. Cleve. *Clin. J. Med.* **2009**, *76*, 49.
- Alzheimer, A. *Gesamte Neurol. Psychiatr.* **1911**, *4*, 356–385.
- Yankner, B. A. *J. Neuron.* **1996**, *16*, 921.
- Maqbool, M.; Mobashir, M.; Hoda, N. *Eur. J. Med. Chem.* **2016**, *107*, 63.
- Bar-On, P.; Millard, C. B.; Harel, M.; Dvir, H.; Enz, A.; Sussman, J. L.; Silman, I. *Biochemistry* **2002**, *41*, 3555.
- Bourne, Y.; Radic, Z.; Sulzenbacher, G.; Kim, E.; Taylor, P.; Marchot, P. *J. Biol. Chem.* **2006**, *281*, 29256.
- Inestrosa, N. C.; Alvarez, A.; Pérez, C. A.; Moreno, R. D.; Vicente, M.; Linker, C.; Casanueva, O. I.; Soto, C.; Garrido, J. *Neuron* **1996**, *16*, 881.
- Dinamarca, M. C.; Sagal, J.; Quintanilla, R. A.; Godoy, J. A.; Arrázola, M. S.; Inestrosa, N. C. *Mol. Neurodegener.* **2010**, *5*, 1326–5–4.
- Giacobini, E. *Pharmacol. Res.* **2004**, *50*, 433.
- Frisardi, V.; Solfrizzi, V.; Imbimbo, P. B.; Capurso, C.; D'Introno, A.; Colacicco, A. M.; Vendemiale, G.; Seripa, D.; Pilotto, A.; Capurso, A.; Panza, F. *Curr. Alzheimer Res.* **2010**, *7*, 40.
- Hardy, J. *Trends Neurosci.* **1997**, *20*, 154.
- Bonda, D. J.; Wang, X.; Perry, G.; Nunomura, A.; Tabaton, M.; Zhu, X.; Smith, M. A. *Neuropharmacology* **2010**, *59*, 290.
- Ono, K.; Hasegawa, K.; Naiki, H.; Yamada, M. *J. Neurosci. Res.* **2004**, *75*, 742.
- Gholivand, K.; Hosseini, Z.; Farshadian, S.; Naderi-manesh, H. *Eur. J. Med. Chem.* **2010**, *45*, 5130.
- Gamba, D.; Liberato, C.; Pisoni, S.; Amorim, D.; Antonio, M.; Lunardi, P.; Alberto, C.; Gonçalves, S. *Eur. J. Med. Chem.* **2010**, *45*, 526.
- Singh, U. P.; Bhat, H. R.; Gahtori, P. *J. Mycol. Médicale/J. Med. Mycol.* **2012**, *22*, 134.
- Corbett, T. H.; Leopold, W. R.; Dykes, D. J.; Roberts, B. J.; Griswold, D. P.; Schabel, F. M. *Cancer Res.* **1982**, *42*, 1707.
- Bhat, H. R.; Singh, U. P.; Gahtori, P.; Ghosh, S. K.; Gogoi, K.; Prakash, A.; Singh, R. K. *RSC Adv.* **2013**.
- Lozano, V.; Aguado, L.; Hoorelbeke, B.; Renders, M.; Camarasa, M.-J.; Schols, D.; Balzarini, J.; San-f, A.; Perez-P, M. *J. Med. Chem.* **2011**, *120*, 5335–5348.
- Gahtori, P.; Ghosh, S. K.; Singh, B.; Singh, U. P.; Bhat, H. R.; Uppal, A. *Saudi Pharm. J.* **2012**, *20*, 35.
- Kumar, D.; Khan, S. I.; Ponnann, P.; Rawat, D. S. *New J. Chem.* **2014**, *38*, 5087.
- Naz, H.; Jameel, E.; Hoda, N.; Shandilya, A.; Khan, P.; Islam, A.; Ahmad, F.; Jayaram, B.; Hassan, M. I. *Bioorg. Med. Chem. Lett.* **2016**, *26*, 782.
- Helmja, K.; Vaher, M.; Pussa, T.; Kaljurand, M. *J. Chromatogr. A* **2009**, *1216*, 2417.
- Jayaram, B.; Singh, T.; Mukherjee, G.; Mathur, A.; Shekhar, S.; Shekhar, V. *BMC Bioinformatics* **2012**, *13*, S7.
- Singh, T.; Biswas, D.; Jayaram, B. *J. Chem. Inf. Model.* **2011**, *51*, 2515.
- Gupta, A.; Gandhimathi, A.; Sharma, P. J. B. *Protein Pept. Lett.* **2007**, *14*, 632.
- Ellman, G.; Courtney, K.; Andres, V.; Feather-stone, R. *Biochem. Pharmacol.* **1961**, *7*, 88.
- Cheng, B.; Gong, H.; Xiao, H.; Petersen, R. B.; Zheng, L.; Huang, K. *Biochim. Biophys. Acta* **2013**, *1830*, 4860.
- Levine, H. *Protein Sci.* **2008**, *2*, 404.
- Inestrosa, N. C.; Dinamarca, M. C.; Alvarez, A. *FEBS J.* **2008**, *275*, 625.
- Dávalos, A.; Gómez-Cordovés, C.; Bartolomé, B. *J. Agric. Food Chem.* **2003**, *51*, 2512.
- Maalej, E.; Chabchoub, F.; Oset-Gasque, M. J.; Esquivias-Pérez, M.; González, M. P.; Monjas, L.; Pérez, C.; de los Ríos, C.; Rodríguez-Franco, M. I.; Iriepa, I.; Moraleda, I.; Chioua, M.; Romero, A.; Marco-Contelles, J.; Samadi, A. *Eur. J. Med. Chem.* **2012**, *54*, 750.
- Choi, J.-S.; Braymer, J. J.; Nanga, R. P. R.; Ramamoorthy, A.; Lim, M. H. *Proc. Natl. Acad. Sci.* **2010**, *107*, 21990.
- Yang, F.; Lim, G. P.; Begum, A. N.; Ubeda, O. J.; Simmons, M. R.; Ambegaokar, S. S.; Chen, P. P.; Kaye, R.; Glabe, C. G.; Frautschy, S. A.; Cole, G. M. *J. Biol. Chem.* **2005**, *280*, 5892.
- Mosmann, T. *J. Immunol. Methods* **1983**, *65*, 55.
- Vellonen, K.-S.; Honkakoski, P.; Urtti, A. *Eur. J. Pharm. Sci.* **2004**, *23*, 181.
- Szczepanik, A. M.; Funes, S.; Petko, W.; Ringheim, G. E. *J. Neuroimmunol.* **2001**, *113*, 49.
- Schrödinger LLC. QikProp, version 3.5. New York 2012.
- Pearlman, D. A.; Case, D. A.; Caldwell, J. W.; Ross, W. S.; Cheatham, T. E.; DeBolt, S.; Ferguson, D.; Seibel, G.; Kollman, P. *Comput. Phys. Commun.* **1995**, *91*, 1.
- Jain, T.; Jayaram, B. *FEBS Lett.* **2005**, *579*, 6659.
- Petersen, E. F.; Goddard, T. D.; Huang, C. C.; Couch, G. S.; Greenblatt, D. M.; Meng, E. C.; Ferrin, T. E. *J. Comput. Chem.* **2004**, *25*, 1605.
- Bolognesi, M. L.; Andrisano, V.; Bartolini, M.; Banzi, R.; Melchiorre, C. *J. Med. Chem.* **2005**, *48*, 24.
- Wang, R.-G.; Zhu, X.-Z. *Brain Res.* **2003**, *961*, 131.